Supporting Information

Acetylacetone Functionalized Periodic Mesoporous Organosilicas: from Sensing to Catalysis

Chunhui Liu[a,b,c], Mahdieh Haghighat[a], Himanshu Sekhar Jena[a], Dirk Poelman[b], Nathalie De Geyter[d], Rino Morent[d], Anna M. Kaczmarek[c], and Pascal Van Der Voort[a]**

[a]COMOC - Center for Ordered Materials Organometallics and Catalysis, Department of Chemistry, Ghent University, Krijgslaan 281 S3, 9000 Ghent;

[b]Lumilab, Department of Solid State Sciences, Ghent University, Krijgslaan 281 S1, 9000 Ghent;

[c]NanoSensing Group, Department of Chemistry, Ghent University, Krijgslaan 281 S3, 9000 Ghent

[d]RUPT - Research Unit Plasma Technology, Department of Applied Physics, Ghent University, St-Pietersnieuwstraat 41 B4, 9000 Ghent

** Corresponding authors: Email: Anna.Kaczmarek@UGent.be; Email: Pascal.VanDerVoort@UGent.be*

Table S 1 The comparisons of the sensing performance for different nanoparticle fluorometric sensors in aqueous solution.

Fluorescence probe	Materials	Analytes detected	Linear range	K_{sv} (M^{-1})	LOD	Ref
NS-CQDs	carbon quantum dots (CQDs)	Cu^{2+}	0 – 1 μM	-	1.65 μM	1
SiO_2/CdS NCs	nanocrystals	Cu^{2+}	0 – 3 μM	-	3.5×10^{-2} μM	2
ZCM microsphere	QD composite	Cu^{2+}, Cr^{2+}, Fe^{3+}	0 – 1 μM	3.85×10^{5}	1.6×10^{-5} μM	3
CE/11-MUA-AuNCs	gold nanoclusters	Cu^{2+}, Cd^{2+}, Zn^{2+}	0.05–10 μM	-	0.026 μM	4
AIEgens fabricated on nanoscale ZIF-8	aggregation-induced emission luminogens with MOFs	Cu^{2+}	0 – 0.1 μM	-	5.5×10^{-4} μM	5
$[Ce(1,5\text{-}NDS)_{1.5}(H_2O)_5]_n$	MOFs	Cu^{2+}	5 - 100 μM	7668	3 μM	6
AuNCs/PQD@SiO_2	gold nanocomposites	Cu^{2+}	0 - 160 μM	4400	3 μM	7
QG-scaffolded COFs	COFs	Cu^{2+}	0.0032 - 32 μM	-	5×10^{-4} μM	8
$[Eu(bpdc)_{1.5}(H_2O)_2]_n$	Eu-MOFs	Fe^{3+}, Cu^{2+}, PO_4^{3-}	0 – 400 μM	3240	33 μM	9
$\{[Eu(L)(DMF)(H_2O)]\cdot 0.5DMF\}_n$	Eu-MOFs	Cu^{2+}	0.01 - 1000 μM	4.3×10^{4}	1.02×10^{3} μM	10
$[Eu(L)(DEF)(H_2O)]_n$	Eu-MOFs	Cu^{2+}	0.01 - 1000 μM	5.7×10^{4}	5×10^{4} μM	
Eu-MOFs (4, 40-AZ, DMF and H_3BTC)	Eu-MOFs	Cu^{2+}	2 - 1000 μM	2.9×10^{4}	1.395 μM	11
$\{[Tb(HL)]\cdot 3DMF\cdot 3H_2O\}n$ (LZG-Tb)	Tb-MOFs	Cu^{2+}	0 - 0.25 μM	8.2×10^{6}	1.65×10^{-3} μM	12
$\{[Eu(HL)]\cdot 3DMF\cdot 3H_2O\}n$ (LZG-Eu)	Eu-MOFs	Cu^{2+}	0 - 0.25 μM	4.9×10^{6}	1.35×10^{-3} μM	
TH-PMO-100	PMOs	Cu^{2}	0.1 - 1 μM	1.6×10^{4}	40 μM	13
RSPMOs	PMOs	Cu^{2}	0.1 - 1 μM	-	0.1 μM	14
SCN-PMO	PMOs	Cu^{2}	8.75 - 20 μM	-	0.67 μM	15
Ag-PMO-YS	nanocomposites	Cu^{2}	0.1 - 9 μM	-	0.02 μM	16
$Eu(NTA)_3$L-COOH-PMO	Eu-PMOs	Cu^{2}	0 - 20 μM	2.5×10^{6}	0.046 μM	17
ePMO@Eu_PA	Eu-PMOs	Cu^{2}	0 - 400 μM	2100	35.2 μM	18
acac(20)-PMO@Eu_tta	Eu-PMOs	Cu^{2}	0 - 2.5 μM	1.8×10^{5}	0.108 μM	This work

Table S 2 Comparison of the acac-PMO catalyst with other $VO(acac)_2$ based catalysts.

Entry	Catalyst	Reaction conditions	Yield (%)	TON[a]	Ref
1	$VO(acac)_2$	catalyst (10 mol %), CH_2Cl_2, reflux, 8 h	92	9.2	19
2	VO-TAPT-2,3-DHTA COF	catalyst (35 mg, 0.97 mmol/g V), DCM, 40 ℃, 12 h	98	29	20
3	VO-PyTTA-2,3-DHTA COF	catalyst (35 mg, 0.77 mmol/g V), DCM, 40 ℃, 12 h	96	36	20
3	V@acac-CTF	catalyst (40 mg, 0.306 mmol/g V), DCM, 40 ℃, 8 h	95	213	21
4	acac(100)-PMO@VO_acac	catalyst (15 mg, 0.59 mmol/g V), DCM, 40 ℃, 12 h	98	111	This work

[a] TON = turnover number

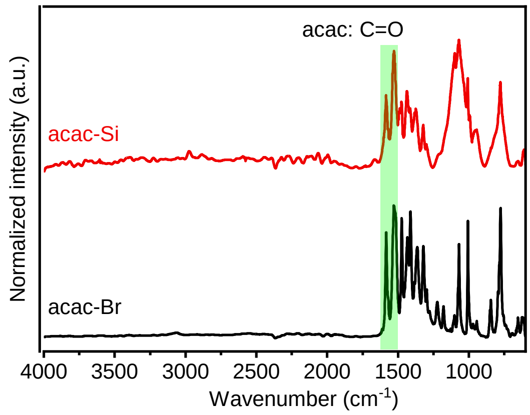

Figure S1. FT-IR spectra of acac-Br and acac-Si.

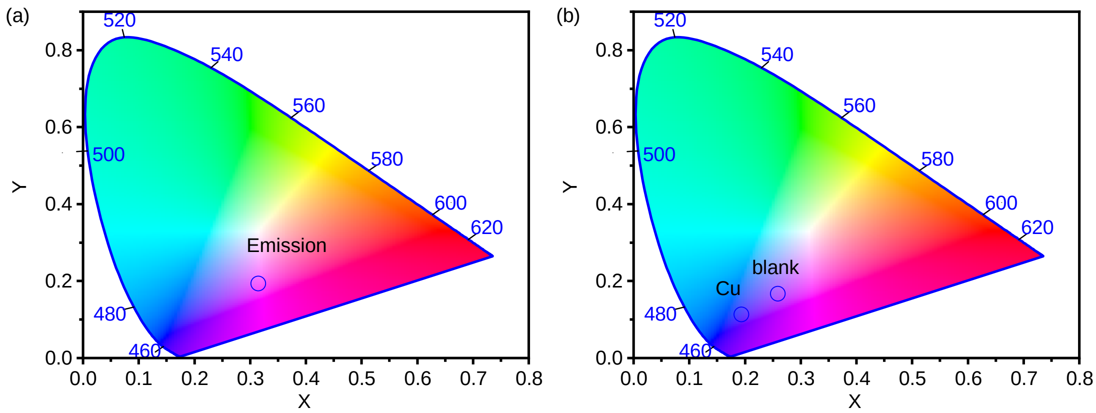

Figure S2. CIE chromaticity diagram of (a) solid acac(20)-PMO@Eu_tta; (b) colloidal suspensions of acac(20)-PMO@Eu_tta with and without Cu^{2+}.

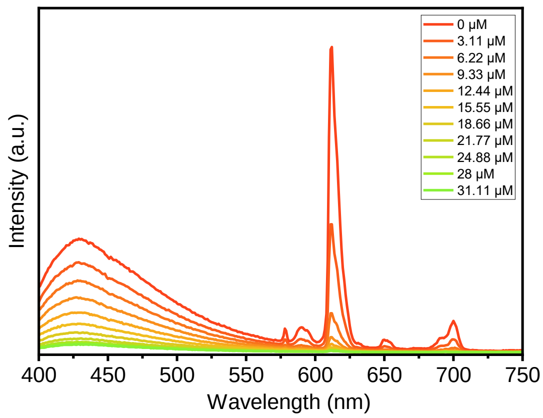

Figure S3. Luminescence spectra of acac(20)-PMO@Eu_tta under different concentrations of Cu^{2+} aqueous solutions.

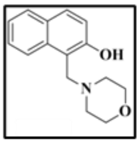

^{1}H NMR (300 MHz, δ(ppm), $CDCl_3$): 7.76 (d, J = 8.7 Hz, 1H), 7.69 (d, J = 7.5 Hz, 1H), 7.63 (d, J = 9.0 Hz, 1H), 7.40-7.35 (m, 1H), 7.24-7.18 (m, 1H), 7.04 (d, J = 9.0 Hz, 1H), 4.08 (s, 2H), 3.7 (br, 4H), 2.6 (br, 4H).

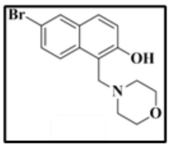

^{1}H NMR (300 MHz, δ (ppm), $CDCl_3$): 7.8 (d, J = 2.1 Hz, 1H), 7.58 (d, J = 9.0 Hz, 1H), 7.5 (d, J = 9.0 Hz, 1H), 7.40 (dd, J = 9.0, 2.1 Hz, 1H), 7.01 (d, J = 9.0 Hz, 1H), 4.01 (s, 2H), 3.7 (br, 4H), 2.56 (br, 4H).

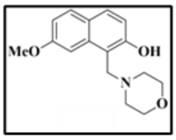

^{1}H NMR (300 MHz, δ (ppm), $CDCl_3$): 7.6 (d, J = 8.9 Hz, 1H), 7.53 (d, J = 8.8 Hz, 1H), 7.18 (s, 1H), 7.02 (d, J = 2.2 Hz, 1H), 6.9 (d, J = 2.4 Hz, 1H), 4.01 (s, 2H), 3.85 (s, 3H), 3.72 (br, 4H), 2.62 (br, 4H).

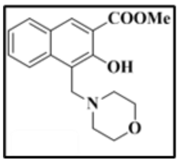

^{1}H NMR (300 MHz, δ (ppm), $CDCl_3$): 8.43 (s, 1H), 7.74 (d, J = 8.2 Hz, 1H), 7.61 (d, J = 8.4 Hz, 1H), 7.46-7.41 (m, 1H), 7.28-7.23 (m, 1H), 3.95 (s, 5H), 3.71-3.62 (m, 4H), 2.57-2.41 (m, 4H).

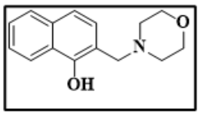

^{1}H NMR (300 MHz, δ (ppm), $CDCl_3$): 8.30-8.26 (m, 1H), 7.76-7.74 (m, 1H), 7.49-7.43 (m, 2H), 7.30 (d, J = 8.2 Hz, 1H), 7.04 (d, J = 8.2 Hz, 1H), 4.02 (s, 2H), 3.80- 3.76 (m, 4H), 2.56 (br, 4H).

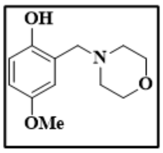

^{1}H NMR (300 MHz, δ (ppm), $CDCl_3$): 7.86 (d, J = 8.6 Hz, 1H), 7.66 (d, J = 7.4 Hz, 1H), 6.8 (d, J = 8.2 Hz, 1H), 3.8 (s, 2H), 3.69 (br, 4H), 2.46 (br, 4H).

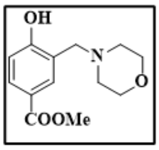

^{1}H NMR (300 MHz, δ (ppm), $CDCl_3$): 7.83 (d, J = 8.2 Hz, 1H), 7.62 (d, J = 6.8 Hz, 1H), 6.96 (d, J = 8.2 Hz, 1H), 3.80 (s, 3H), 3.7 (s, 2H), 3.62 (br, 4H), 2.42 (br, 4H).

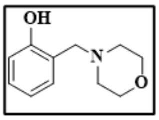

^{1}H NMR (300 MHz, δ (ppm), $CDCl_3$): 7.18 (d, J = 8.2, 1H), 7.13 (t, J = 8.2 Hz, 1H), 6.92 (d, J = 7.6 Hz, 1H), 6.82- 6.77 (m, 1H), 3.62 (s, 2H), 3.66 (br, 4H), 2.5 (br, 4H).

Figure S4. ^{1}H-NMR data of Mannich-reaction product in $CDCl_3$.

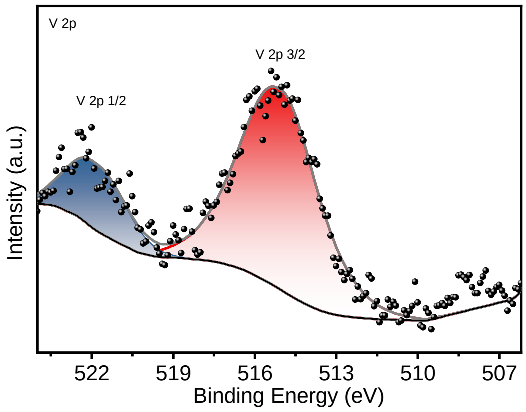

Figure S5. Deconvoluted XPS spectra of vanadium in the V 2p region for acac(100)-PMO@VO_acac catalyst.

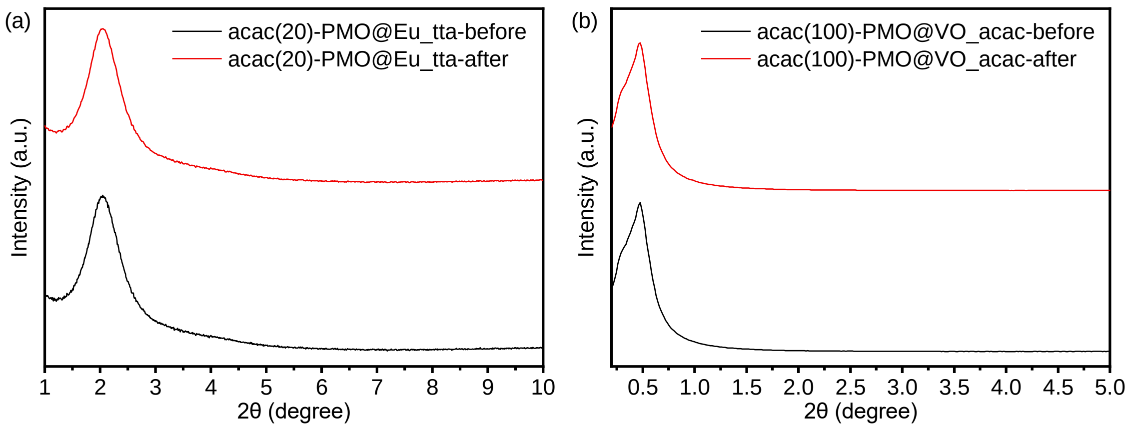

Figure S6. (a) XRD patterns of acac(20)-PMO@Eu_tta before and after immersing in water with Cu^{2+} ions and (b) XRD patterns of acac(100)-PMO@VO_acac before and after catalysis.

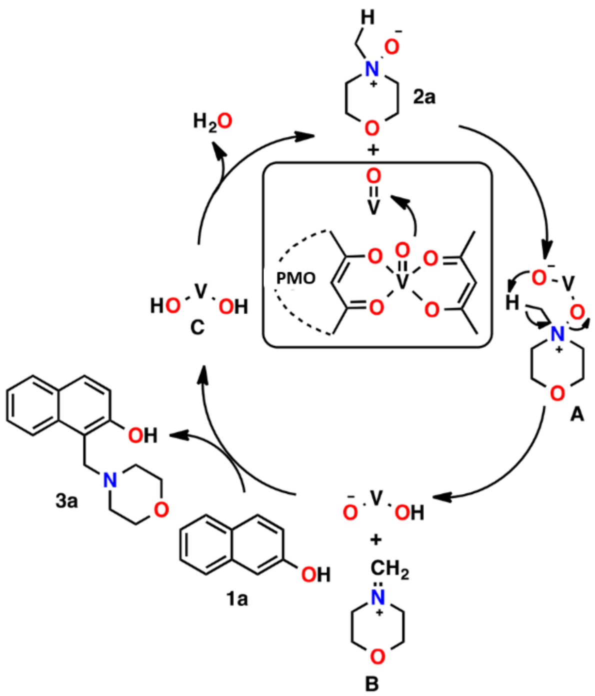

Scheme S 1 Proposed mechanism of Mannich-type reaction catalyzed by acac(100)-PMO@VO_acac.

References

1. N. Chaudhary, P. K. Gupta, S. Eremin and P. R. Solanki, J. Environ. Chem. Eng., 2020, 8, 103720.

2. T. Xie, X. Zhong, Z. Liu and C. Xie, Mikrochim. Acta, 2020, 187, 323.

3. M. M. R. Khan, T. Mitra and D. Sahoo, RSC Adv, 2020, 10, 9512-9524.

4. M. L. Desai, H. Basu, S. Saha, R. K. Singhal and S. K. Kailasa, J. Mol. Liq., 2020, 304, 112697.

5. S. Xie, Q. Liu, F. Zhu, M. Chen, L. Wang, Y. Xiong, Y. Zhu, Y. Zheng and X. Chen, J Mater Chem C, 2020, 8, 10408-10415.

6. S. Geranmayeh, M. Mohammadnejad and S. Mohammadi, Ultrason Sonochem, 2018, 40, 453-459.

7. W. Xue, J. Zhong, H. Wu, J. Zhang and Y. Chi, Analyst, 2021, 146, 7545-7553.

8. Y. Y. Cai, Y. Jiang, L. P. Feng, Y. Hua, H. Liu, C. Fan, M. Y. Yin, S. Li, X. X. Lv and H. Wang, Anal. Chim. Acta, 2019, 1057, 88-97.

9. Z. D. Li, Z. Y. Zhan, Y. J. Jia, Z. Li and M. Hu, J Ind Eng Chem, 2021, 97, 180-187.

10. R. R. Ma, Z. W. Chen, S. N. Wang, Q. X. Yao, Y. W. Li, J. Lu, D. C. Li and J. M. Dou, J Solid State Chem, 2017, 252, 142-151.

11. J. C. Zhou, Y. H. Chen, S. Xian, Y. C. Liang, G. J. Huang, L. Wang and X. Z. Yang, J Solid State Chem, 2021, 304, 122542.

12. Z. G. Lin, F. Q. Song, H. Wang, X. Q. Song, X. X. Yu and W. S. Liu, Dalton Trans., 2021, 50, 1874-1886.

13. M. Gao, S. Han, Y. Hu and L. Zhang, J. Phys. Chem. C, 2016, 120, 9299-9307.

14. X. Y. Qiu, S. H. Han and M. Gao, J. Mater. Chem. A, 2013, 1, 1319-1325.

15. M. Gao, C. Xing, X. Jiang, L. Xu, P. Li and C. D. Hsiao, J. Lumin., 2021, 36, 951-957.

16. L. Yang, S. Shen, J. Zhu, Y. Zhang, Y. Lin, J. Wang, F. Tao, L. Wang and J. Zhang, ACS Appl. Nano Mater., 2023, 6, 1910-1918.

17. H. Li, Y. J. Li, Z. Zhang, X. L. Pang and X. D. Yu, Mater Design, 2019, 172, 107712.

18. W. Liu, A. M. Kaczmarek, H. Rijckaert, P. Van Der Voort and R. Van Deun, Dalton Trans, 2021, 50, 11061-11070.

19. D. R. Hwang and B. J. Uang, Org. Lett., 2002, 4, 463-466.

20. H. Vardhan, L. X. Hou, E. Yee, A. Nafady, M. A. Al-Abdrabalnabi, A. M. Al-Enizi, Y. X. Pan, Z. Y. Yang and S. Q. Ma, Acs Sustain Chem Eng, 2019, 7, 4878-4888.

21. H. S. Jena, C. Krishnaraj, G. B. Wang, K. Leus, J. Schmidt, N. Chaoui and P. Van der Voort, Chem. Mater., 2018, 30, 4102-4111.